Journal of Renewable Energy and Environment

Research Article

Journal Homepage: www.jree.ir

Applying Sliding-Mode Control to a Double-Stage Single-Phase Grid-Connected PV System

Seyed Ali Akbar Fallahzadeh[a], Navid Reza Abjadi[a*], Abbas Kargar[a], Frede Blaabjerg[b]

[a] *Faculty of Technology and Engineering, Shahrekord University, Shahrekord, Chaharmahal and Bakhtiari, Iran.*
[b] *Department of Energy Technology, Aalborg University, Aalborg, Denmark.*

PAPER INFO

Paper history:
Received 09 June 2020
Accepted in revised form 20 September 2020

Keywords:
Sliding Mode,
POSLLC,
Grid Connected,
Photovoltaic

ABSTRACT

This study investigates a new double-stage single-phase Grid-Connected (GC) Photo-Voltaic (PV) system. This PV system includes a DC-DC Positive Output Super Lift Luo Converter (POSLLC) and a single-phase inverter connected to a grid through an RL filter. Due to its advantages, the POSLLC was used between PV panel and inverter instead of the conventional boost converter. The state space equations of the system were solved. By using two Sliding Mode Controls (SMCs), PV panel voltage and POSLLC inductor current were controlled and the designed controls were compared. Two of these SMCs included a simple Sign Function Control (SFC) and a conventional SMC. To control the power injected into the grid with a unity power factor, an SMC was used. Perturb and Observe (P&O) method was employed to reach maximum power of the PV panel. The Maximum Power Point Tracking (MPPT) control generated the voltage reference of the PV panel. Similar controls were used for the boost converter instead of POSLLC. The obtained results were compared.

https://doi.org/10.30501/jree.2020.233358.1114

1. INTRODUCTION

Among the available renewable energy resources, PV energy, which enjoys low cost and government support, is used more and more every day. Energy harvesting from PV panels is quite dependent on solar irradiation and temperature. Elaborate control methods should be used along with Maximum Power Point Tracking (MPPT) to achieve maximum power extraction [1].

A PV system can work in the off-grid or on-grid mode [2]. The use of grid-tie or on-grid PV systems is increasing nowadays [3]. Usually, grid-tie PV systems are characterized by two stages of conversion [4-5]. Two-stage conversion is generally required because of the very high voltage conversion ratio [6]. Industry has shown that this topology can achieve more than 96 % efficiency [7]. In the first stage, a DC-DC converter is used and, in the second stage, an inverter is connected to the grid. Failure to apply the DC-DC converter to the single-phase grid-connected PV system causes some difficulties such as double-frequency power ripple and inverter input voltage fluctuations [8]. Recently, the application of single-phase grid-connected PV systems has attracted considerable attention because there are many residential and commercial customers for single-phase grid-connected PV systems, which generate extra PV energy for some hours a day [1]. Such advanced applications require precise control.

DC-DC converters are applied to many commercial and industrial equipment. The main objective of these converters is to ensure high conversion voltage ratio, high efficiency, and high-power density. To increase the gain of a conventional DC-DC boost converter in renewable energy applications, cascade boost converters [9, 10] or double boost converters are used; however, such topologies are complicated and, thus, need sophisticated control techniques. In fact, these converters have many inductors and capacitors (or semiconductor switches) that promote the order of the system.

Recently, a family of DC-DC converters, called Luo converters, has received notable attention and one of the most remarkable DC-DC converters in this family is POSLLC [11-13]. In fact, there are three types of Luo converter: elementary circuit, re-lift circuit, and triple-lift circuit. The analysis of POSLLCs in different operation modes was conducted in [14]. One of the main indices of DC-DC converters is their efficiency. Vinoth and Ramesh [15] compared the efficiency rates of Luo and Boost converters in a hybrid grid-connected topology based on photovoltaic system and permanent magnet synchronous generator. They found that the efficiency of the system that used Luo converter was 5 % higher than the system with a boost converter. Narmadha et al. [16] proposed a stand-alone PV system based on POSLLC and controlled the

*Corresponding Author's Email: navidabjadi@yahoo.com (N.R. Abjadi)
URL: http://www.jree.ir/article_114504.html

Please cite this article as: Fallahzadeh, S.A.A., Abjadi, N.R., Kargar, A. and Blaabjerg, F., "Applying sliding-mode control to a double-stage single-phase grid-connected PV system", ***Journal of Renewable Energy and Environment (JREE)***, Vol. 8, No. 1, (2021), 1-12. (https://doi.org/10.30501/jree.2020.233358.1114).

output voltage. Gnanavadivel et al. [17] incorporated Lou converter in the AC-DC converter to improve power factor.

Classical linear control is usually used to achieve the control objectives of GC solar PV systems [18]. Linear controllers are unable to achieve the desired control objectives at different operating points, i.e. under fast-changing weather conditions [19]. In [20], a double-stage PV system using DC-DC Buck converter was presented. Two-cascade Proportional Resonant (PR) controllers were used to control the injected current into the grid. In [21], two PI controllers were employed to control the current injected to the grid and the panel voltage in a two-stage system connected to a single-phase utility grid. In [22], a double-stage PV system using DC-DC boost converter was presented. Conventional PI controls were used and a high-order observer was proposed. PI and fuzzy control of output voltage for a POSLLC was presented in [16]. The drawbacks of these plans include the difficulty of adjusting the parameters of controllers and the inability of linear controllers to fast track the voltage reference in the event of a change in weather conditions. Using nonlinear control can be advantageous for overcoming the problems associated with different operating points in GC PV systems [23-26]. There are different types of current nonlinear control schemes for PV systems such as SMC [23, 24], feedback linearization control [25, 27], and backstepping control [28]. Nonlinear control of output voltage for a POSLLC using an observer-based scheme was presented in [29]. The nonlinear control proposed in [29] was characterized by a complicated structure, which made its tuning difficult. In [30], by using a boost converter in a PV system, the output voltage was controlled, which is not suitable for MPPT purposes; moreover, the stabilty of internal dynamic was not investigated. In [31], a robust backstepping controller was designed for a buck boost DC-DC converter in a PV system which has a complicated structure to implement. In [32], the control of a stand-alone PV system consisting of a POSLLC was presented, and an ohmic load was fed by the PV system. In [33], two controllers were used to optimize the PV energy injected into the three-phase grid. The first controller was used to predict the DC voltage that would allow the three-phase inverter to track the maximum power point of photovoltaic generator under variable climatic conditions and variable load. This new controller used a multivariate polynomial interpolation based on Lagrange's theory. The second controller was based on the robust SMC. It was used to control the active and reactive powers injected into the network. This system was of single-stage type and the contollers were cascaded, not independent. Therefore, failure to set one controller can have a negative effect on the other controller and thus on the system as a whole. In [34], an adaptive fuzzy SMC was designed for a boost converter in a PV system; by using fuzzy conrtol, there is no guaranty for the overall system stability and the process of design is complicted.

In the current study, POSLLC and a prototype of the single-phase inverter are suggested for transferring the power of a PV panel to the grid. PV panel voltage, inductor current of DC- DC converter, and injected current to the grid are controlled to achieve maximum power and high performance. Since the POSLLC works in the lower range of duty cycles, parasitic effects and losses are reduced to minimum and a highly efficient operation is achieved.

PV panels have nonlinear characteristics and are expensive. It is indispensable to extract the maximum power from PV panels. Providing voltage through PV panel and the connected circuit depends on climate conditions and the operating point. In this condition, an MPPT algorithm is necessary to provide reference voltage for PV panel. SMC is a robust method that shows significant tracking effectiveness and provides a swift reaction to climate changes. In [24], a simple sign function control was used to control the DC link voltage of POSLLC. In this study, the DC link voltage was controlled by two nonlinear control methods and the methods were compared using POSLLC and boost converter. Voltage gain of POSLLC was higher and, at the same time, its average inductor current was lower than those of other conventional converters. Consequently, POSLLC is widely popular in higher power applications. Furthermore, it has an additional capacitor that strictly regulates output voltage. To control the current injected to the grid, an SMC method was also applied and the commands for the inverter switches were produced. To obtain the maximum power from the panel, the P&O MPPT technique was used. The main innovations of this paper include (a) the application of DC-DC POSLLC to a single-phase double-stage grid-connected PV system that outperforms other similar systems with DC-DC boost converter and (b) simultaneous nonlinear controlling of the injected current to the grid and the DC-DC converter capacitor voltage. To confirm the advantages of the proposed PV system and controllers, simulation software with PSIM module at different irradiation rates and temperatures is presented and discussed.

2. PV SYSTEM STRUCTURE

Fig. 1 shows the overall double-stage PV system. The DC side contains PV panel connected to capacitor C_{pv} and POSLLC. AC side contains the inverter, RL filter, and utility grid.

2.1. Positive output super lift Luo converter

Fig. 2 illustrates the elementary circuit of POSLLC, its equivalent circuit when the switch S is closed (on), and its equivalent circuit when the switch S is open (off).

According to Fig. 2-b, C_1 is charged on V_{in} while switch S is on. Because L_1 and C_1 are parallel, the current of inductor L_1 (i_{L_1}) experiences an increase. In the switched-off mode, as shown in Fig. 2-c, the voltage across inductor L_1 becomes $-(V_o-2V_{in})$ and hence, i_{L_1} is reduced.

The average of the inductor voltages is zero in a steady state. It is assumed that DT_s is the switch-on period and $(1-D)T_s$ is the switch-off period. Therefore, the Voltage Gain (VG) of the POSLLC is obtained through the following relation [13]:

$$VG=\frac{V_o}{V_{in}}=\frac{2-D}{1-D} \quad (1)$$

Let C_1 and V_{C_1} be a large value and a constant, respectively, as given in Vin= V_{C_1}. The average model of the POSLLC in Continuous Conduction Mode (CCM) is expressed as follows [5]:

$$\dot{i}_{L_1} = \frac{1}{L_1}(2v_{in} - v_O + (v_O - v_{in})D)$$
$$\dot{v}_O = \frac{1}{C_2}(i_{L_1} - \frac{v_O}{R} - i_{L_1}D) \quad (2)$$

where $D \in (0,1)$.

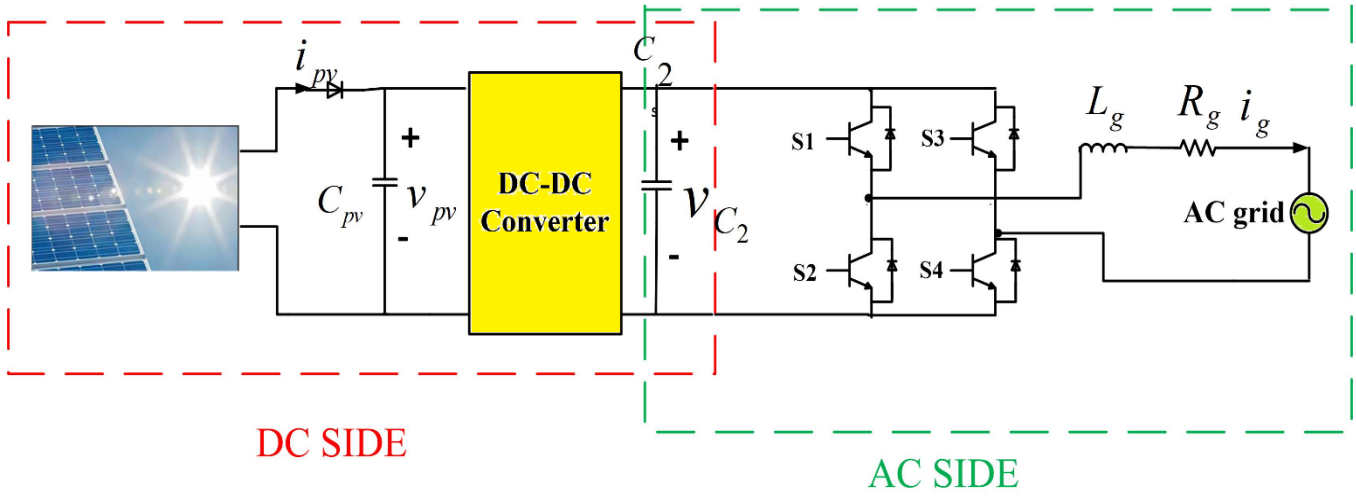

Figure 1. Configuration of the PV system

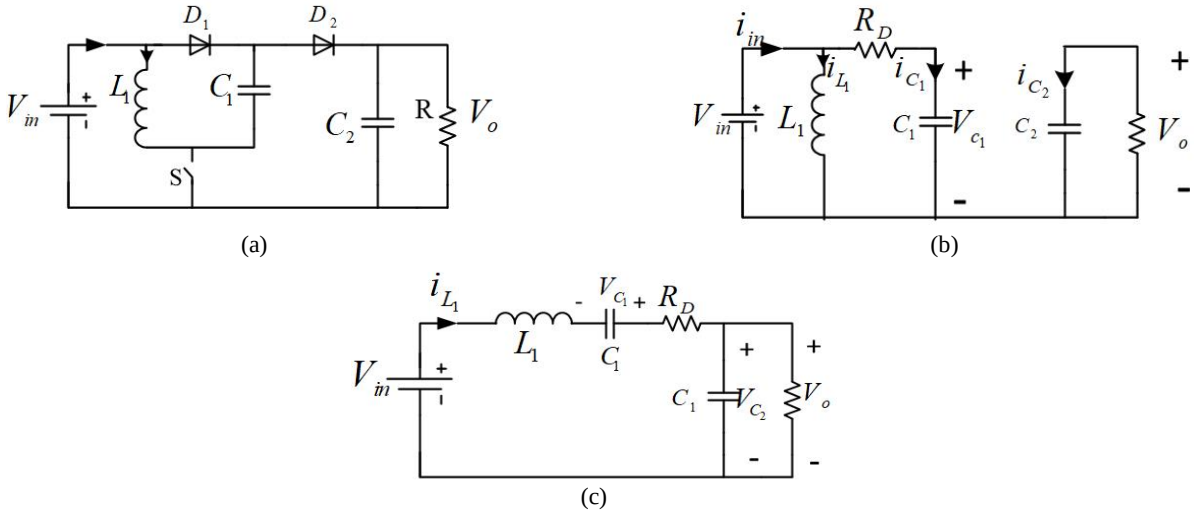

Figure 2. (a) Elementary circuit diagram, (b) Equivalent circuit when switch is on, and (c) Equivalent circuit when switch *S* is off

2.2. DC side model

According to Relation (2), the overall DC side state variables shown in Fig. 1 and their state equations are well defined as follows:

$$x=[i_{L_1} \; v_{pv} \; v_{C_1} \; v_o]^T \quad (3)$$

$$\dot{X}=\begin{bmatrix} \frac{-R_D}{L_1} & \frac{1}{L_1} & \frac{1}{L_1} & \frac{-1}{L_1} \\ \frac{-R_D}{C_{pv}} & 0 & 0 & 0 \\ \frac{1}{C_1} & 0 & 0 & 0 \\ \frac{1}{C_2} & 0 & 0 & \frac{-1}{RC_2} \end{bmatrix} X + \begin{bmatrix} \frac{-v_{C_1}}{L_1} + \frac{i_{L_1}R_D}{L_1} + \frac{v_{C_2}}{L_1} \\ \frac{-v_{C_1}}{C_{pv}R_D} - \frac{v_{pv}}{C_{pv}R_D} \\ \frac{-v_{pv}}{C_1R_D} - \frac{v_{C_1}}{C_1R_D} - \frac{i_L}{C_1} \\ -\frac{i_{L_1}}{C_2} \end{bmatrix} u(t) + \begin{bmatrix} 0 \\ \frac{i_{pv}}{C_{pv}} \\ 0 \\ 0 \end{bmatrix} \quad (4)$$

The voltage of capacitor C_2 is controlled using a PI controller, as shown in Fig. 3 and regulated into its reference value. Therefore, (4) is reduced to a second-order equation as follow:

$$\dot{z}=\begin{bmatrix} \frac{-R_D}{L_1} & \frac{1}{L_1} \\ \frac{-1}{C_{pv}} & 0 \end{bmatrix} z + \begin{bmatrix} \frac{-v_{C_1} + i_{L_1}R_D + v_o}{L_1} \\ \frac{v_{C_1} - v_{pv}}{C_{pv}R_D} \end{bmatrix} u(t) + \begin{bmatrix} \frac{v_{C_1} - v_o}{L_1} \\ \frac{i_{pv}}{C_{pv}} \end{bmatrix} \quad (5)$$

where

$$z=[i_{L_1} \; v_{pv}]^T \quad (6)$$

The above equation is written in the following compact canonical form:

$$\dot{z}=f(z)+g(z)u(t) \quad (7)$$

where

$$f(z)=\begin{bmatrix}\frac{-R_D}{L_1} & \frac{1}{L_1}\\ \frac{-1}{C_{pv}} & 0\end{bmatrix}z+\begin{bmatrix}\frac{V_{C_1}-V_o}{L_1}\\ \frac{i_{pv}}{C_{pv}}\end{bmatrix}=\begin{bmatrix}\frac{-R_D i_{L_1}+v_{pv}+V_{C_1}-V_o}{L_1}\\ \frac{-i_{L_1}+i_{pv}}{C_{pv}}\end{bmatrix}$$

$$g(z)=\begin{bmatrix}\frac{-V_{C_1}+i_{L_1}R_D+V_o}{L}\\ \frac{V_{C_1}-V_{pv}}{C_{pv}R_D}\end{bmatrix} \quad (8)$$

2.3. AC side model

The AC side including an H-bridge inverter and an LR filter is connected to the utility grid. As shown in Fig. 1, the switch positions are represented by the simple input command χ of switches as follows:

$$\chi=+1 \ \text{if } S_1,S_4:\text{on}, S_2,S_3:\text{off}$$
$$\chi=-1 \ \text{if } S_2,S_3:\text{on}, S_1,S_4:\text{off} \quad (9)$$

when $\chi=+1$, the state equations can be written as follows:

$$\dot{v}_o=\frac{1}{C_2}(-i_g+i_o)$$
$$\dot{i}_g=\frac{1}{L_g}(-i_g R_g+v_i+e_g) \quad (10)$$

The grid voltage is assumed to be sinusoidal given by:

$$e_g=V_m \sin\omega t \quad (11)$$

when $\chi=-1$, the state equations can be given as follows:

$$\dot{v}_o=\frac{1}{C_2}(i_g+i_o)$$
$$\dot{i}_g=\frac{-1}{L_g}(i_g R_g+v_i+e_g) \quad (12)$$

Combining relations (10) and (12), one can obtain:

$$\dot{v}_o=\frac{1}{C_2}(-i_g r(t)+i_o)$$
$$\dot{i}_g=\frac{1}{L_g}(-i_g R_g+v_i r(t)-e_g) \quad (13)$$

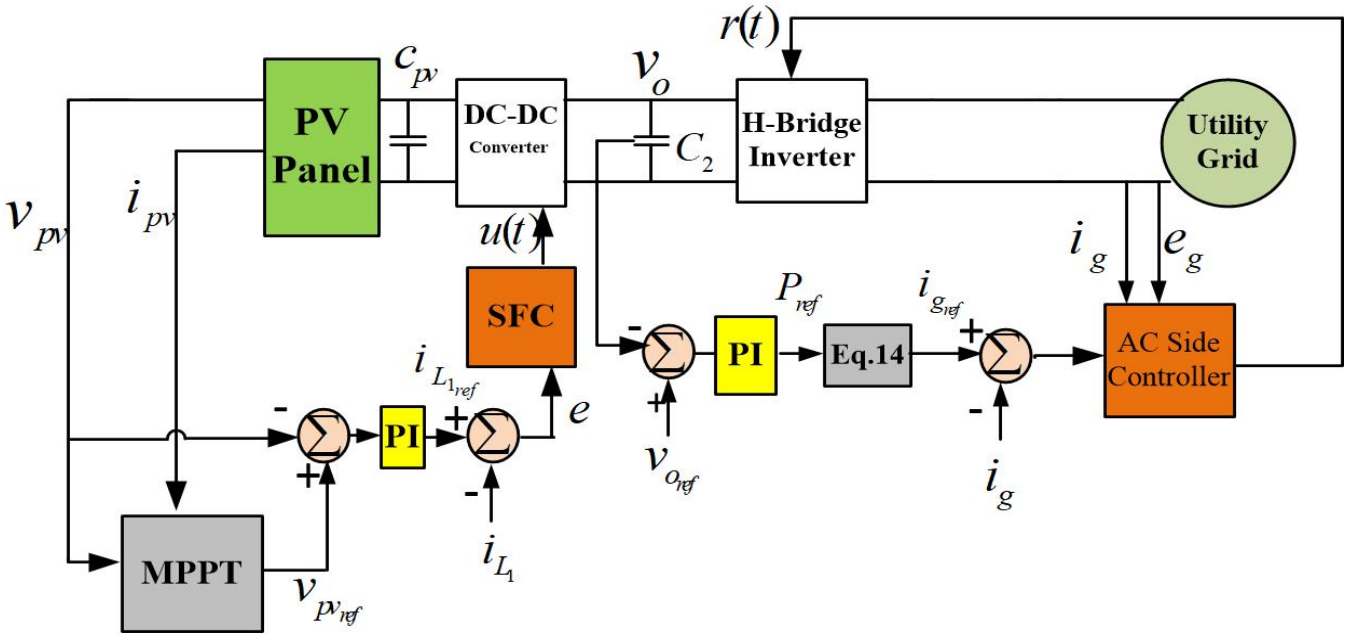

Figure 3. Shematic block-diagram of the proposed controller using SFC

3. CONTROL OF SYSTEM

3.1. AC side controller

The total schematic block diagram of the PV system is shown in Fig. 3. The DC side includes POSLLC and capacitor C_{pv}. The ratio of reference current to the current injected to the grid ($i_{g_{ref}}$) is a function of the active power reference (P_{ref}), which is given in [35]:

$$\dot{i}_{g_{ref}}=\frac{2P_{ref}}{V_m}\sin\omega t \quad (14)$$

where P_{ref} is obtained using a PI controller. The input to the PI controller is the difference between the output voltage of DC-DC converter and its reference.

The error between the actual value of grid current(i_g) and its reference is considered as a sliding variable:

$$\sigma(x,t)=i_g-i_{g_{ref}}=i_g-\frac{2P_{ref}}{V_m}\sin\omega t \quad (15)$$

The control input, r(t) , is obtained as follows:

$$\sigma(x,t)=0 \ \text{and} \ \dot{\sigma}(x,t)=\dot{i}_g-\dot{i}_{g_{ref}}=0 \quad (16)$$

Substituting (13) into (16), one obtains the following:

$$r(t)=\frac{1}{v_i}\left(\frac{2P_{ref}L_g\omega\cos\omega t}{V_m}+e_g+R_g i_g\right)+b\,\mathrm{sgn}(\sigma) \quad (17)$$

where sgn(σ) is the sign function aimed at achieving robustness in the face of parametric uncertainties in the control law and b is a positive constant.

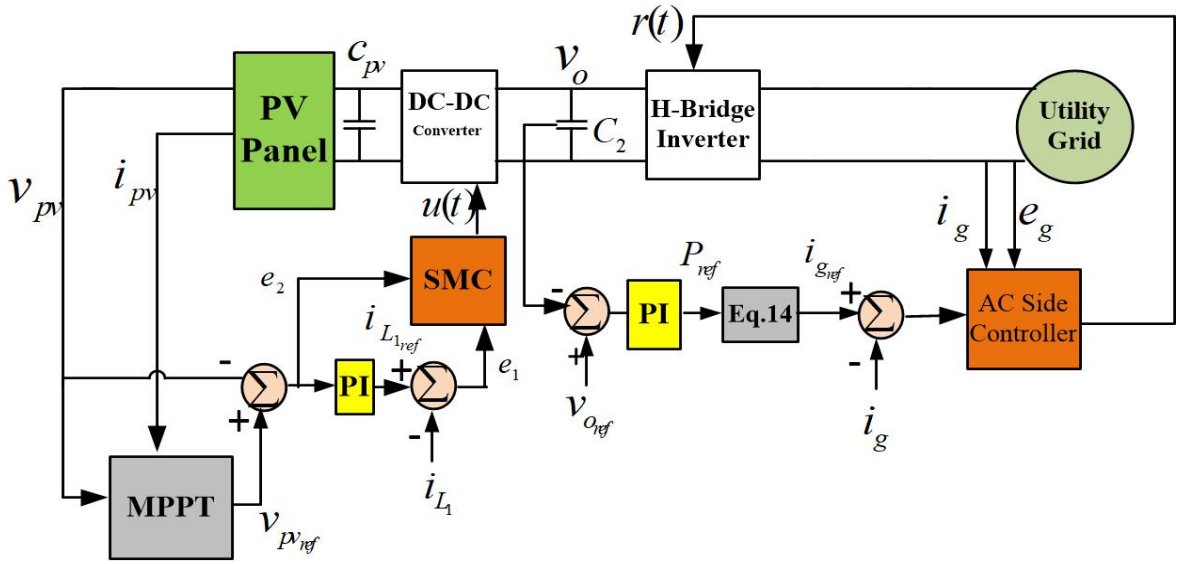

Figure 4. Shematic diagram of the proposed controller using conventional SMC

3.2. DC side control using Sign Function Control (SFC)

Consider the following sliding variable for inductor current:

$$e(z)=i_{L_1}-i_{L_{1ref}} \quad (18)$$

where $i_{L_{1ref}}$ is the reference value of i_{L_1} obtained by comparing PV panel voltage v_{pv} with its reference $v_{pv_{ref}}$ using a Proportional Integrator (PI) controller. One can drive the output function e(z) to zero through discontinuous control, indicating that i_{L_1} converges to its desired value. The Lie derivative theory is applied in the following manner [36]:

$$L_f e(z)=\frac{\partial e(z)}{\partial z_1}f_1(z)+\frac{\partial e(z)}{\partial z_2}f_2(z)=\frac{-R_D i_{L_1}+v_{pv}+V_{C_1}-V_o}{L}$$
$$L_g e(z)=\frac{\partial e(z)}{\partial z_1}g_1(z)+\frac{\partial e(z)}{\partial\partial z_2}g_2(z)=\frac{-V_{C_1}+i_{L_1}R_D+V_o}{L} \quad (19)$$

where f_1 and f_2 are the rows of $f(z)$ and g_1 and g_2 are the rows of $g(x)$. $L_f e(z)$ is the Lie derivative of e(z) with respect to f(z).

The equivalent control is obtained as follows:

$$u(z)=-\frac{L_f e(z)}{L_g e(z)}=\frac{R_D i_L-v_{pv}+V_{C_1}-V_o}{-V_{C_1}+i_{L_1}R_D+V_o} \quad (20)$$

Fig. 3 shows the block diagram of the proposed controller.

3.3. DC side control using Sliding Mode Controller (SMC)

In this section, a conventional sliding mode control is designed to control the inductor current i_{L_1} and the capacitor voltage V_{pv}, as shown in Fig. 4. The following sliding variable is defined for this purpose:

$$s_2(z,t)=K_1e_1+K_2e_2 \quad (21)$$

where K_1 and K_2 are positive constants and e_1 and e_2 are defined as follows:

$$e_1=i_{L_{1ref}}-i_{L_1}$$
$$e_2=v_{pv_{ref}}-v_{pv} \quad (22)$$

By substituting (5) into the following equation, the control law of POSLLC can be obtained as in (24):

$$\dot{s}_2(z,t)=K_1\dot{e}_1+K_2\dot{e}_2=0 \quad (23)$$

$$u(t)=\frac{-K_1\left(\dot{i}_{L_{ref}}+\frac{R_D i_L-v_{pv}-v_{c_1}+v_o}{L}\right)-K_2\left(\dot{v}_{pv_{ref}}+\frac{i_L-i_{PV}}{C_{pv}}\right)}{K_1\left(\frac{v_{c_1}-R_D i_L-v_o}{L}\right)+K_2\left(\frac{v_{pv}-v_{c_1}}{C_{pv}R_D}\right)}+K_3\,\mathrm{sgn}(s_2) \quad (24)$$

where K_3 is a positive constant.

4. SIMULATION AND DISCUSSION

The simulation results show the performance of the proposed controls in handling the GC single-phase PV system and DC-DC converters. Table 1 shows technical specifications of the PV panel. The step time for simulation and switching frequency are considered as $1\mu s$ and 20 KHz, respectively. The Pulse Width Modulation (PWM) technique is applied to the case of a single-phase inverter.

4.1. Comparison of two SMC strategies

In Fig. 3, the POSLLC is controlled using SFC method to achieve MPPT by regulating the PV panel voltage. Fig. 4 shows the DC-DC converter control by conventional SMC with the sliding variable given in (15). Table 2 shows the parameter values of POSLLC.

Table 1. PV panel parameters and specifications

Reference cell temperature	25 °C
Maximum power	110 W
Number of cells	72
Voltage at maximum power	34.8 V
Open-circuit voltage	43.4 V
Standard light intensity at 25 °C	1000 w/m^2
Short circuit current	3.4 A
Current at maximum power	3.16 A

Table 2. DC-DC converters, RL filter, and input capacitor values

Boost converter values	L_1	0.2 mH
	C_1	0.2 mF
POSLLC values	L_1	0.2 mH
	C_1	0.1 mF
	C_2	0.1 mF
RL filter values	L_g	5 mH
	R_g	50 mΩ
Input capacitor value	C_{pv}	0.1 mF

The simulation results of this section were affected by the variations in radiation and temperature. The characteristic of output power of the PV panel was dependent on sun irradiation and ambient temperature.

The output characteristics of PV cells or modules are commonly represented by the current–voltage (I–V) and power–voltage (P–V) curves. In some special cases, voltage–current (V–I) and power–current (P–I) curves were used to represent the PV output characteristics [37]. Standard Test Conditions (STC) are conditions in which the solar modules are tested in a laboratory. Module testing is carried out in the following conditions: solar radiation intensity of 1000 W/m^2, optical air mass of AM 1.5, temperature of solar module of 25 °C, and wind speed of 1 m/s [38]. Figs. 5 and 6 include Power-Voltage (P-V) curves of PV panel at different irradiances and temperatures, respectively. Figs. 7 and 8 display Current-Voltage (I-V) curves of the panel under different conditions.

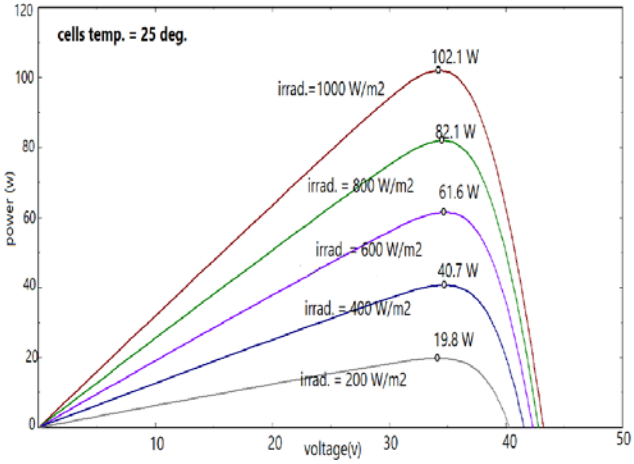

Figure 5. Power-voltage curves at different irradiances (T=25 °C)

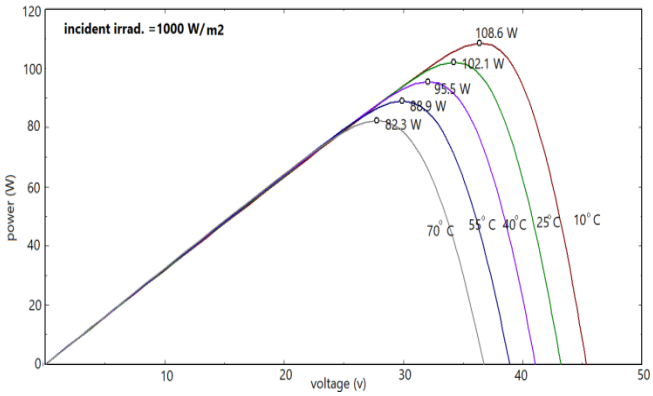

Figure 6. Power-voltage curves at different tempartures (G=1000 W/m^2)

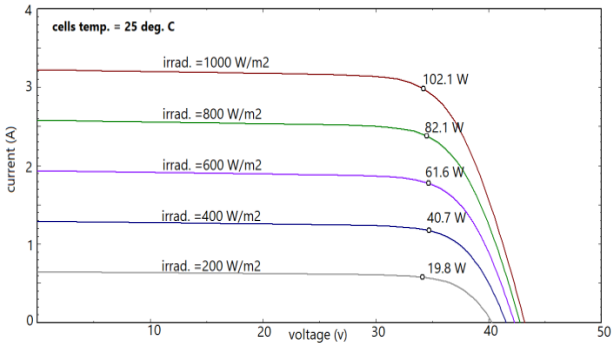

Figure 7. I-V curves at different irradiances (T=25 °C)

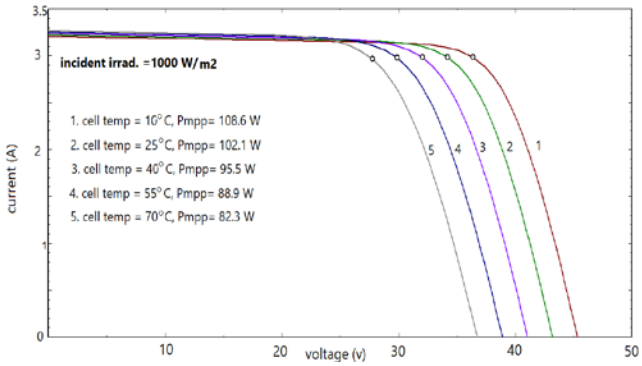

Figure 8. I-V curves at different temperatures (G=1000 W/m^2)

Figs. 9-15 compare the simulation results for the PV system using SFC and SMC at different values of irradiance and temperatures including T=25 °C. The value of irradiance G increases from 800 to 1200 W/m^2 at t=0.2 s and is reduced from 1200 to 1000 W/m^2 at t=0.4 s, as shown in Fig. 9. According to Fig. 6, when irradiation steps up, the obtained PV power increases, which, in turn, elevates the amplitude of the injected current to the grid. The POSLLC inductor current will also increase. These results are shown in Figs. 10-14. Besides, according to Figs. 11 and 14, the MPPT technique at different values of radiation shows a suitable performance.

Fig. 10 shows the function of AC side controller in tracking the injected current to the utility grid and its reference at different irradiance values. A comparison between SFC and SMC in the DC side controller is made and given in Figs. 11 and 12. Fig. 11 shows that voltage fluctuations around the reference in SMC are fewer in number than those in SFC. In

addition, SMC has better performance for input capacitor C_{pv} (shown in Fig. 1) and ensures longer life of C_{pv}. Fig. 12 compares SMC-based inductor current with SFC-based inductor current. The SFC method has better functionality than SMC because the former is subject to less fluctuations and a lower average value.

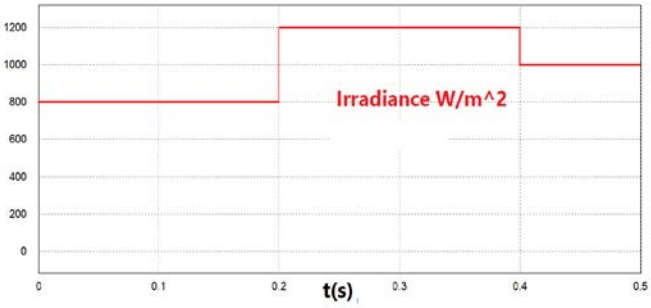

Figure 9. Irradiance changes of the PV panel

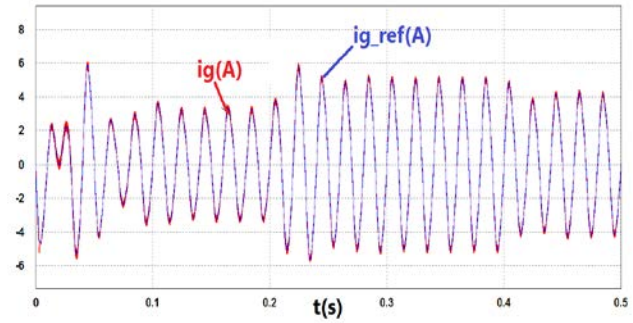

(a)

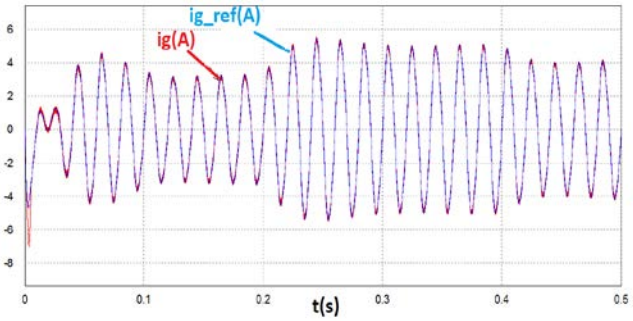

(b)

Figure 10. Grid current and its reference at different values of irradiance using (a) SFC and (b) SMC

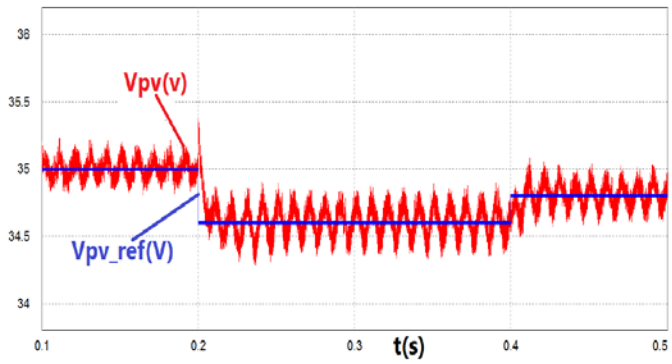

(a)

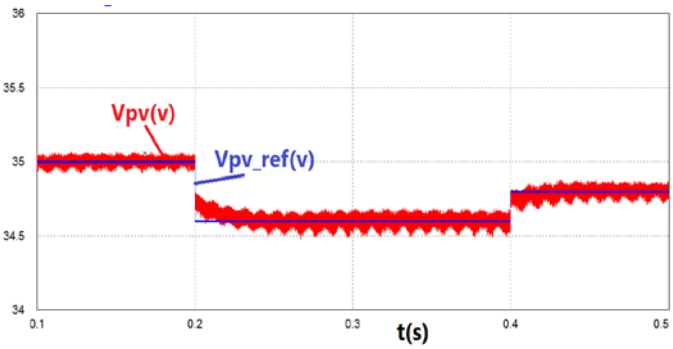

(b)

Figure 11. PV extracted voltage and its reference at different values of irradiance using (a) SFC and (b) SMC

Fig. 13 compares maximum power with delivered power of the PV panel. This figure demonstrates that MPPT method has proper performance using both of the proposed controllers despite different radiation values. Fig. 14 shows how the PV panel current varies due to irradiance changes. The PV panel current using SMC is more acceptable than that using SFC. Satisfactory Unity Power Factor (UPF) with respect to the power supply network is proven, as shown in Fig. 15, which shows utility grid voltage and injected current to the grid.

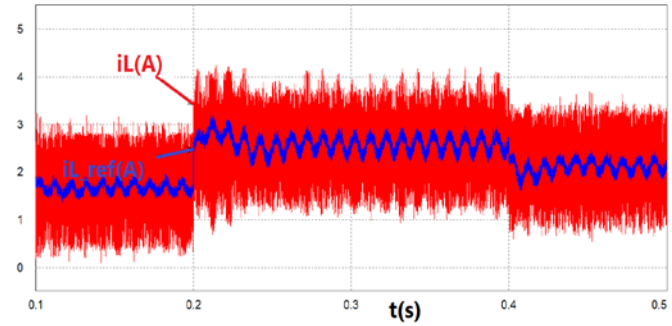

(a)

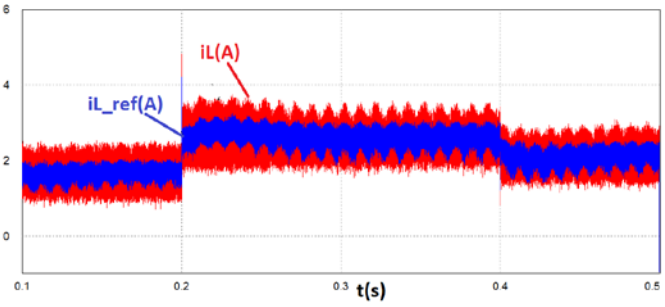

(b)

Figure 12. POSLLC inductor current and PV current at different values of irradiance using (a) SFC and (b) SMC

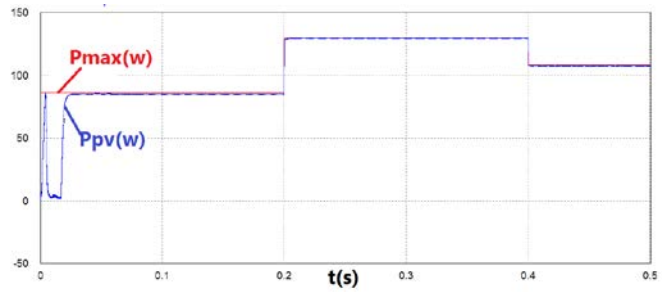

(a)

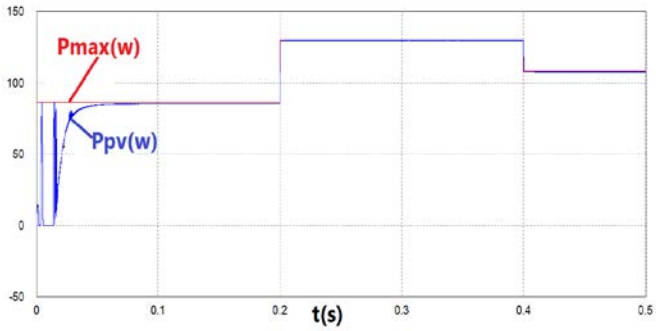

(b)

Figure 13. Maximum power and delivered power of PV panel at different values of irradiance using (a) SFC and (b) SMC

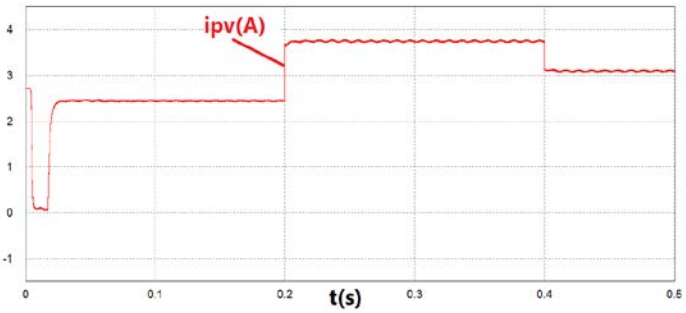

(a)

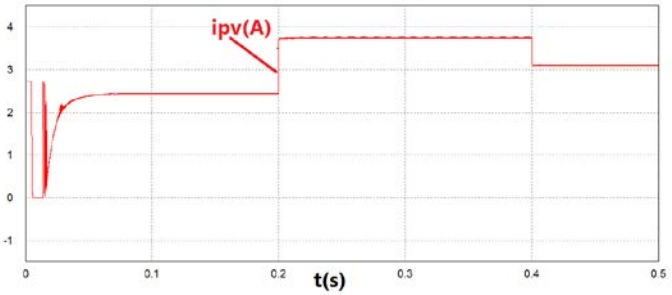

(b)

Figure 14. Delivered PV panel current at different values of irradiance using (a) SFC and (b) SMC

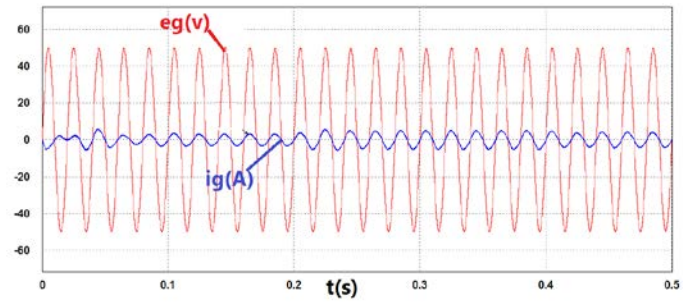

(a)

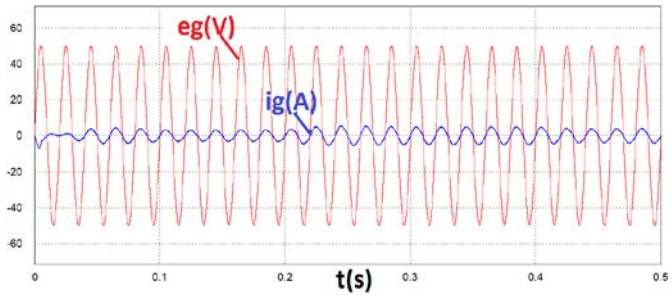

(b)

Figure 15. UPF checking by (a) SFC and (b) SMC

This study carried out another experiment at temperature T ranging from 25 °C to 40 °C at t=0.25 s (Fig. 16) and irradiance G=1000 W/m^2 using the controllers (Figs. 3 and 4). The simulation results of the proposed controllers are presented and compared in Figs. 17 to 20. According to Fig. 6, as the temperature of the PV panel decreases, the extracted power increases. By increasing the temperature of PV panel, the its voltage is reduced and current increases, as shown in Figs. 17 and 19, respectively. At varying temperatures, SMC outperforms SFC. Figs. 17-18 show that the fluctuations of inductor current of DC-DC converter and PV voltage panel in the system using SMC are less than those in the system using SFC. These fluctuations increase the efficiency and lifespan of capacitor C_{pv} in the system using SMC.

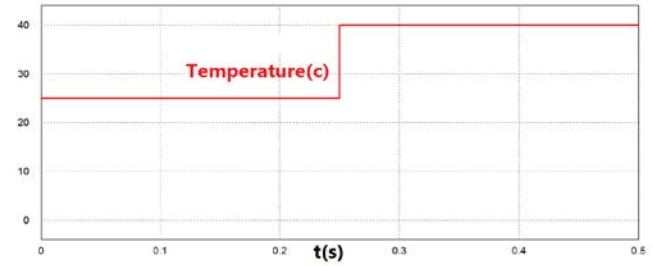

Figure 16. Temperature changes of PV panel

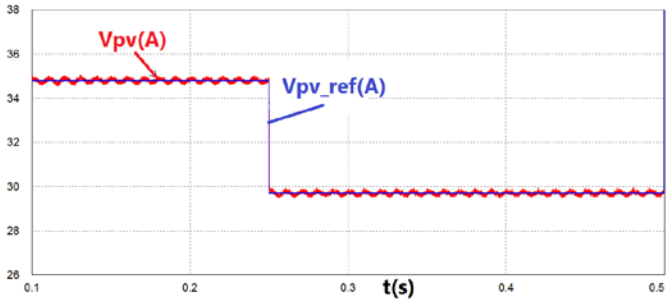

(a)

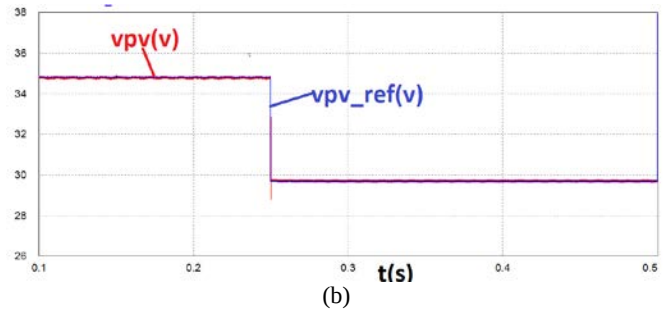

(b)

Figure 17. PV extracted voltage and its reference at different temperatures using (a) SFC and (b) SMC

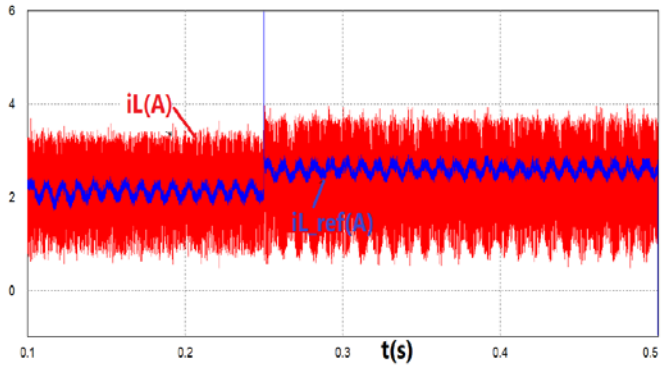

(a)

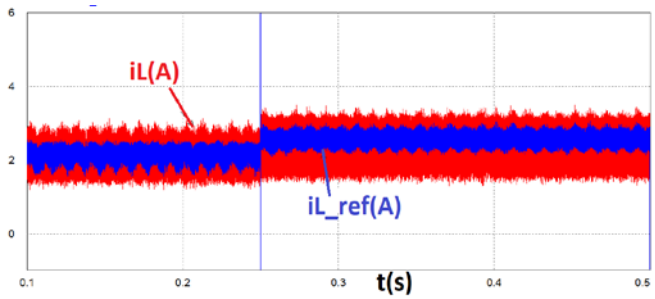

(b)

Figure 18. POSLLC inductor current using (a) SFC and (b) SMC

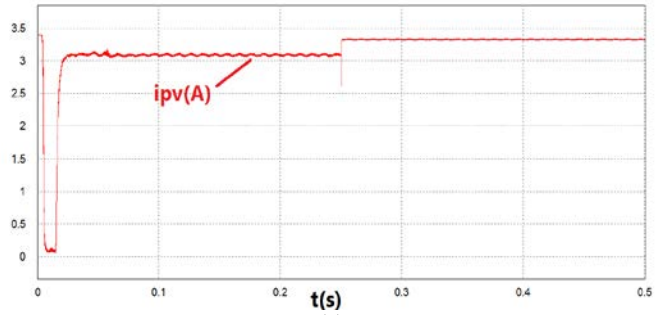

(a)

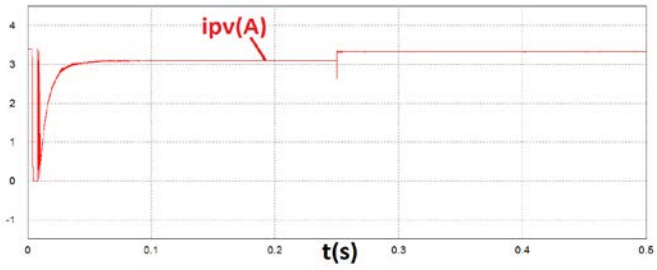

(b)

Figure 19. Unity power factor checking by (a) SFC and (b) SMC

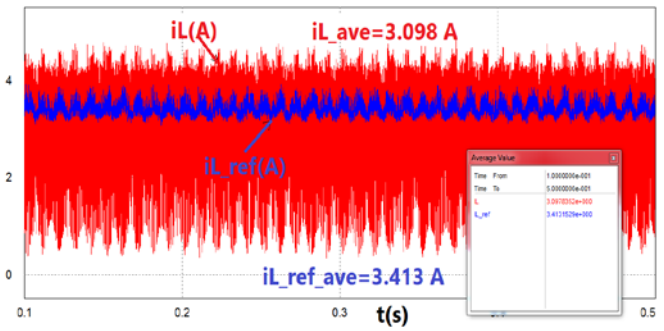

(a)

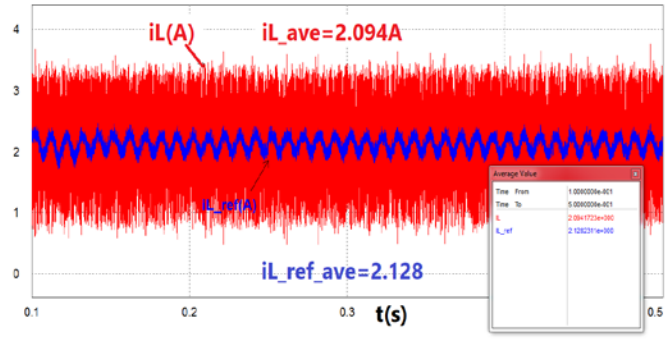

(b)

Figure 20. Inductor current and its reference: (a) the proposed system using boost converter and (b) the proposed system using POSLLC

4.2. Comparison of performances of POSLLC and boost converter in the proposed system

In this section, the performances of DC-DC, POSLLC, and boost converter in the PV system are compared. Besides its higher voltage gain than the boost converter, POSLLC enjoys another advantage, to be presented later in the paper. Table 2 shows the parameters of the DC-DC boost converter. The inductor value of the boost converter is set equal to the output value 'one' of the POSLLC and the value of its capacitor is equal to the sum of the values of POSLLC capacitors.

Fig. 20-a shows the inductor current of boost converter in the proposed system shown in Fig. 3. The average value of inductor current i_{L_1} is equal to 3.47 A, while the average value of inductor current of the POSLLC in a similar system equals 2.094 A (Fig. 20-b). A lower inductor current value yields lower loss. The proposed system using POSLLC is subject to less voltage fluctuations than the system using boost converter, as shown in Fig. 21, and this ensures the longer lifespan of capacitor C_{pv} using POSLLC. Furthermore, D with POSLLC is less than D with boost converter. Fig. 22-a shows D using POSLLC. The value of D using POSLLC is close to 0.5 (D=0.475), while it equals 0.615 using boost converter (Fig. 22-b). According to Fig. 23, the efficiency of the PV system with boost converter is lower than that of PV system with POSLLC. Input power of both converters is 107.7 W; however, the output power values of POSLLC and boost converter are 105 W and 97.9 W, respectively. Therefore, the POSLLC and the boost converter enjoy efficiency rates of 97.5 % and 90.9 %, respectively, in the same condition.

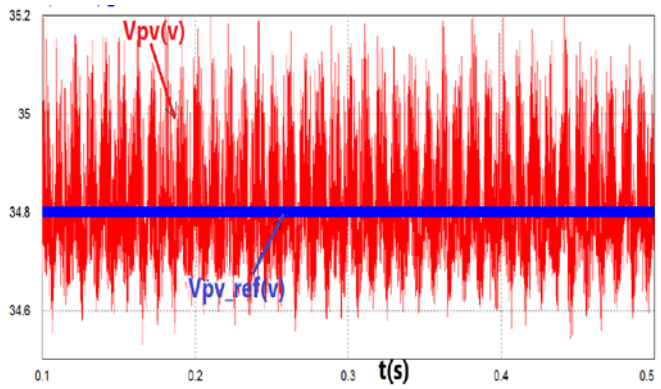

(a)

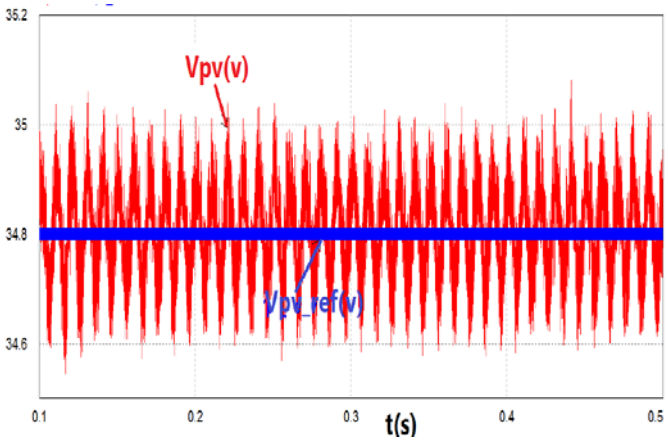

(b)

Figure 21. PV extracted voltage and its reference (zoomed in): (a) the proposed system using boost converter and (b) the proposed system using POSLLC

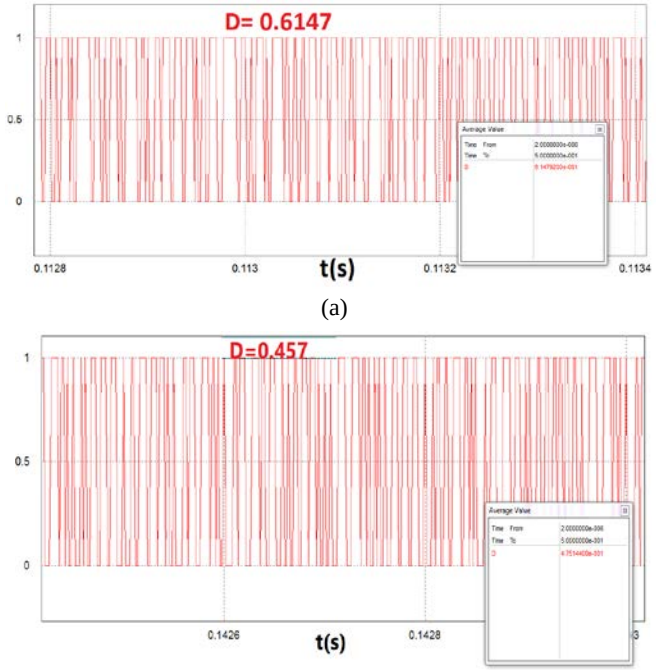

Figure 22. Duty cycle of switching in the proposed system: (a) the proposed system using boost converter and (b) the proposed system using POSLLC

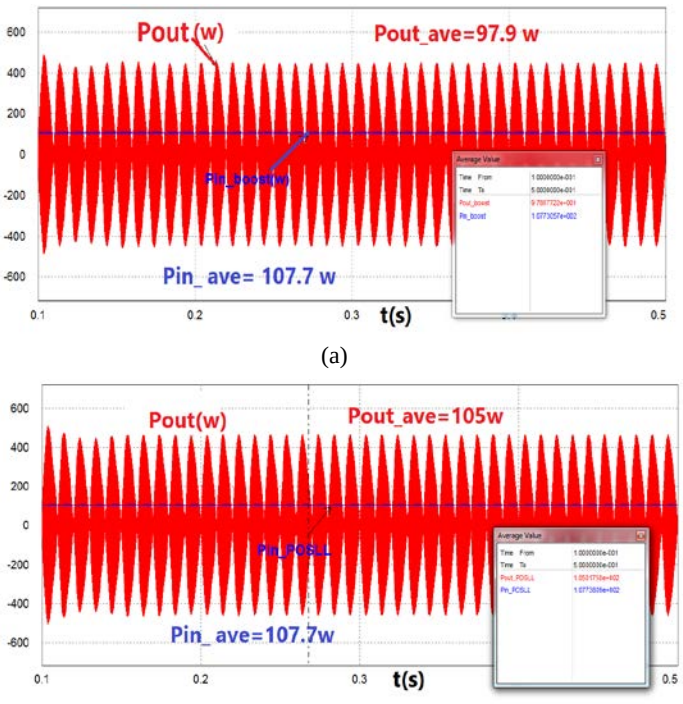

Figure 23. Efficiency comparison of DC-DC converters: (a) the proposed system using boost converter and (b) the proposed system using POSLLC

5. CONCLUSIONS

A new double-stage single-phase GC PV system using POSLLC was presented in this paper. Two nonlinear control methods for input capacitor voltage control in different weather conditions were designed, analyzed, simulated, and compared. Then, the proposed system was investigated from two perspectives. First, the controllers (SFC vs. SMC) and then, the performances of DC-DC converters (POSLLC vs. boost converter) were compared. To control the input capacitor voltage and inductor current of the PV system including POSLLC, SFC and SMC methods were applied. Although the DC side controller using SFC was characterized by a simple structure that enjoyed low cost and ease of use, the comparison of the simulation results illustrated that the SMC had better performance in terms of tracking the reference voltages. Moreover, the fluctuations of the input capacitor voltage and inductor current using SMC were found to be lower, hence promoting the service life of power electronic devices in the system. Table 3 represents a summary of performance comparison and implementation of SFC and SMC.

Another comparison was made between boost converter and POSLLC in the PV system. The simulation results showed that the voltage fluctuation of the input capacitor in the system using POSLLC was lower than that of the input capacitor voltage in the system using boost converter due to the presence of an additional capacitor in the input of POSLLC. Moreover, the average values of inductor current and duty cycle in the system using POSLLC were lower than those in the system using boost converter. The efficiency of POSLLC was found higher than that of boost converter. Furthermore, the unity power factor and MPPT control using P&O method at different temperatures and irradiances were investigated and simulated. The proposed GC PV system using POSLLC with low duty cycle and less ripple will be useful in industrial applications. Table 4 shows a summary of the performance comparison of POSLLC and boost converter in the double-stage grid connected PV system.

Table 3. Performance comparison of the proposed controllers

Description	Using SFC	Using SMC
Grid current reference tracking	Good with fluctuations	Very good
Quality of input voltage tracking	Good with fluctuations	Very good
Practical implementation	Simple	Relatively simple
Operating point area	Very wide	Very wide
Average of inductor current	High	Low
Quality of PV current	Good	Very good
Unity power factor delivery	Excellent	Excellent

Table. 4. Performance comparison of POSLLC and boost converter in the same PV system

Description	Boost converter	POSLLC
Efficiency (%)	90.9	97.5
Average of inductor current (A)	3.098	2.094
Duty cycle of switching	0.61	0.46
Voltage gain considering previous duty cycles	2.56	2.86

6. ACKNOWLEDGEMENT

Authors are grateful to Shahrekord University for the financial support of this study.

NOMENCLATURE

V_{in}, V_o	Average input/output voltage of POSLLC
D	Duty cycle
VG	Voltage gain
T_s	Switching period of POSLLC
V_{in}	Input voltage of POSLLC
R_D	Resistance of diodes D_1 and D_2
V_{pv}, $\mathbf{V}_{pv_{ref}}$	PV panel voltage and its reference
$\mathbf{i}_{L_1}$, $\mathbf{i}_{L_{1_{ref}}}$	POSLLC inductor current and its reference
$\mathbf{V}_{C_1}$	POSLLC capacitor C_1 voltage
R_g, L_g	Resistance and inductance of the filter and the line
V_o, i_o	Output voltage/current of DC-DC converter or input voltage/current of inverter
e_g	Grid voltage
i_g, $i_{g_{ref}}$	Injected current to the grid and its reference
P_{ref}	Reference power delivered to the grid
χ	Inverter switches command
r(t)	Average value of χ in the inverter switching period

REFERENCES

1. Yang, Y. and Blaabjerg, F., "Overview of single-phase grid-connected photovoltaic systems", ***Electric Power Components and Systems***, Vol. 43, No. 12, (2015), 1352-1363. (https://doi.org/10.1080/15325008.2015.1031296).
2. Jafari, M., Ghadamian, H. and Seidabadi, L., "An experimental and comparative analysis of the battery charge controllers in off-grid PV systems", ***Journal of Renewable Energy and Environment (JREE)***, Vol. 5, No. 4, (2018), 46-53. (http://www.jree.ir/&url=http://www.jree.ir/article_95298.html).
3. Rahmani, M., Faghihi, F., Moradi CheshmehBeigi, H. and Hosseini S.M., "Frequency control of islanded microgrids based on fuzzy cooperative and influence of STATCOM on frequency of microgrids", ***Journal of Renewable Energy and Environment (JREE)***, Vol. 5, No. 4, (2018), 27-33. (http://www.jree.ir/article_94119.html).
4. Kjaer, S.B., Pedersen, J.K. and Blaabjerg, F., "A review of single-phase grid-connected inverters for photovoltaic modules", ***IEEE Transactions on Industry Applications***, Vol. 41, No. 5, (2005), 2649-2663. (https://doi.org/10.1109/tia.2005.853371).
5. Fallahzadeh, S.A.A., Abjadi, N.R. and Kargar, A., "Double-stage grid-connected photovoltaic system with POSLL converter using PI resonant controller", ***Proceedings of 5th International IEEE Conference on Control, Instrumentation, and Automation (ICCIA)***, Iran, (2017), 155-160. (https://doi.org/10.1109/icciautom.2017.8258670).
6. Khan, O. and Xiao, W., "An efficient modeling technique to simulate and control submodule integrated PV system for single phase grid connection", ***IEEE Transactions on Sustainable Energy*** ,Vol. 7, No. 1, (2016), 96-107.(https://doi.org/10.1109/tste.2015.2476822).
7. Xiao, W., Edwin, F.F., Spagnuolo, G. and Jatskevich, J., "Efficient approaches for modelingand simulating photovoltaic power systems", ***IEEE Journal of Photovoltaics***, Vol. 3, (2013), 500-508. (https://doi.org/10.1109/jphotov.2012.2226435).
8. Harb, S., Hu, H., Kutkut, N., Batarseh, I. and John Shen, Z., "A three-port photovoltaic (PV) micro-inverter with power decoupling capability", ***Proceedings of 2011 Twenty-Sixth Annual IEEE Applied Power Electronics Conference and Exposition (APEC)***, (2011). (https://doi.org/10.1109/APEC.2011.5744598).
9. Lotfi Nejad, M., Poorali, B., Adib, E. and Motie Birjandi, A.A., "New cascade boost converter with reduced losses", ***IET Power Electronics***, Vol. 9, No. 6, (2016), 1213-1219. (https://doi.org/10.1049/iet-pel.2015.0240).
10. Sosa, J.M., Martinez-Rodriguez, P.R., Vazquez, G. and Nava-Cruz, J.C., "Control design of a cascade boost converter based on the averaged model", ***Proceedings of 2013 IEEE International Autumn Meeting on Power Electronics and Computing (ROPEC)***, (2013). (https://doi.org/10.1109/ROPEC.2013.6702718).
11. Miao, Z. and Luo, F.L., "Analysis of positive output super-lift converter in discontinuous conduction mode", ***Proceedings of 2004 International Conference on Power System Technology***, Singapore, (2004), 828-833. (https://doi.org/10.1109/icpst.2004.1460108).
12. Jiao, Y., Luo, F.L. and Zhu, M., "Generalised modelling and sliding mode control for n-cell cascade super-lift DC-DC converters", ***IET Power Electronics***, Vol. 4, (2011), 532-540. (https://doi.org/10.1049/iet-pel.2010.0049).
13. Luo, F.L. and Ye, H., "Positive output super-lift converters", ***IEEE Transactions on Power Electronics***, Vol. 18, No. 1, (2003), 105-113. (https://doi.org/10.1109/TPEL.2002.807198).
14. Luo, F.L., "Analysis of super-lift Luo-converters with capacitor voltage drop", ***Proceedings of 2008 3rd IEEE Conference on Industrial Electronics and Applications***, Singapore, (2008), 417-422. (https://doi.org/10.1109/iciea.2008.4582550).
15. Vinoth, K. and Ramesh, B., "A modified Luo converter for hybrid energy system FED grid tied inverter", ***International Journal of Engineering and Advanced Technology (IJEAT)***, Vol. 9, No. 1, (2019), 1515-1521. (https://doi.org/10.35940/ijeat.a1288.109119).
16. Narmadha, T.V., Velu, J. and Sudhakar, T.D., "Comparison of performance measures for PV based super-lift Luo-converter using hybrid controller with conventional controller", ***Indian Journal of Science and Technology***, Vol. 9, No. 29, (2016), 1-8. (https://doi.org/10.17485/ijst/2016/v9i29/89937).
17. Gnanavadivel, J., Yogalakshmi, P., Senthil Kumar, N. and Krishna Veni, K.S., "Design and development of single phase AC–DC discontinuous conduction mode modified bridgeless positive output Luo converter for power quality improvement", ***IET Power Electronics***, Vol. 12, No. 11, (2019), 2722-2730. (https://doi.org/10.1049/iet-pel.2018.6059).
18. Selvaraj, J. and Rahim, N.A., "Multilevel inverter for grid-connected PV system employing digital PI controller", ***IEEE Transactions on Industrial Electronics***, Vol. 56, No. 1, (2009), 149-158. (https://doi.org/10.1109/tie.2008.928116).
19. Chowdhury, M.A., "Dual-loop H1 controller design for a grid-connected singlephase photovoltaic system", ***Solar Energy***, Vol. 139, (2016), 640-649. (https://doi.org/10.1016/j.solener.2016.10.039).
20. Bourguiba, I., Houari, A., Belloumi, H. and Kourda, F., "Control of single-phase grid connected photovoltaic inverter", ***Proceedings of 2016 4th International Conference on Control Engineering & Information Technology (CEIT-2016)***, Tunisia, (2016). (https://doi.org/10.1109/ceit.2016.7929116).
21. Sangwongwanich, A., Yang, Y. and Blaabjerg., F., "A sensorless power reserve control strategy for two-stage grid-connected PV systems", ***IEEE Transactions on Power Electronics***, Vol. 32, (2019), 8859-8869. (https://doi.org/10.1109/tpel.2017.2648890).
22. Huang, L., Qiu, D., Xie, F., Chen, Y. and Zhang, B., "Modeling and stability analysis of a single-phase two-stage grid-connected photovoltaic system", ***Energies***, Vol. 10, No. 12, (2017), 1-14. (https://doi.org/10.3390/en10122176).
23. Hao, X., Xu, Y., Liu, T., Huang, L. and Chen, W., "A sliding-mode controller with multiresonant sliding surface for single-phase grid-connected VSI with an LCL filter", ***IEEE Transactions on Power Electronics***, Vol. 28, No. 5, (2013), 2259-2268. (https://doi.org/10.1109/tpel.2012.2218133).

24 Fallahzadeh, S.A.A., Abjadi, N.R., Kargar, A. and Mahdavi. M., "Sliding mode control of single phase grid connected PV system using sign function", ***Proceedings of 2017 IEEE 4th International Conference on Knowledge-Based Engineering and Innovation (KBEI)***, (2017), 391-397. (https://doi.org/10.1109/KBEI.2017.8325009).

25. Mahmud, M.A., Pota, H.R., Hossain, M.J. and Roy, N., "Robust partial feedback linearization stabilization scheme for three-phase grid-connected photovoltaic systems", ***IEEE Transactions on Power Delivery***, Vol. 29, No. 3, (2014), 1221-1230. (https://doi.org/10.1109/jphotov.2013.2281721).
26. Aourir, M., Aboulooifa, A., Lachkar, I., Hamdoun, A., Giri, F. and Cuny, F., "Nonlinear control of PV system connected to single phase grid through half bridge power inverter", ***Proceedings of 20th IFAC***

World Congress, Vol. 50, No. 1, (2017), 741-746. (https://doi.org/10.1016/j.ifacol.2017.08.241).

27. Fallahzadeh S.A.A., Abjadi, N.R. and Kargar, A., "Decoupled active and reactive power control of a grid-connected inverter-based DG using adaptive input-output feedback linearization", ***Iranian Journal of Science and Technology, Transactions of Electrical Engineering***, (2020), 1-10. (https://doi.org/10.1007/s40998-020-00319-3).
28. Roy, T.K., Mahmud, M.A., Hossain, M.J. and Oo, A.M.T., "Nonlinear backstepping controller design for sharing active and reactive power in three phase grid-connected photovoltaic systems", ***Australasian Universities Power Engineering Conference (AUPEC)***, NSW, (2015), 1-6. (https://doi.org/10.1109/aupec.2015.7324866).
29. Mahdavi, M., Shahriari-Kahkehi M. and Abjadi, N.R., "An adaptive estimator-based sliding mode control scheme for Uncertain POESLL converter", ***IEEE Transactions on Aerospace and Electronic systems***, (2019), Vol. 55, No. 6, 3551-3560. (https://doi.org/10.1109/TAES.2019.2908272).
30. Chaibi, Y., Salhi, M. and El-Jouni, A., "Sliding mode controllers for standalone pv systems: Modeling and approach of control", ***International Journal of Photoenergy***, Vol. 2019, (2019), 1-12. (https://doi.org/10.1155/2019/5092078).
31. Ali, K., Khan, L., Khan, Q., Ullah, S., Ahmad, S., Mumtaz, S., Karam, F.W. and Naghmash, A., "Robust integral backstepping based nonlinear mppt control for a pv system", ***Energies***, Vol. 12, No. 16, (2019), 1-20. (https://doi.org/10.3390/en12163180).
32. Fallahzadeh, S.A.A., Abjadi, N.R., Kargar, A. and Blaabjerg. F., "Nonlinear control for positive output super lift Luo converter in stand alone photovoltaic system", ***International Journal of Engineering***, Vol. 33, (2020), 237-247. (https://doi.org/10.5829/ije.2020.33.02b.08).
33. Jendoubia, A., Tlilia, F., and Faouzi Bachaa, F., "Sliding mode control for a grid connected PV-system using interpolation polynomial MPPT approach", ***Elsevier Mathematics and Computers in Simulation,*** Vol. 167, (2020), 208-218. (https://doi.org/10.1016/j.matcom.2019.09.007).
34. Miqoi, S., Ougli, A.E. and Tidhaf, B., "Adaptive fuzzy sliding mode based MPPT controller for a photovoltaic water pumping system", ***International Journal of Power Electronics and Drive System (IJPEDS)***, Vol. 10, No. 1, (2019), 414-422. (https://doi.org/10.11591/ijpeds.v10.i1.pp414-422).
35. Kim, I.S., "Sliding mode controller for the single-phase grid-connected photovoltaic system", ***Applied Energy***, Vol. 83, (2006), 1101-1115. (https://doi.org/10.1016/j.apenergy.2005.11.004).
36. Ramirez H.R. and Ortigoza, R.S., Control design and techniques in power electronics devices, Springer-Verlag, London, (2006). (https://doi.org/10.1007/1-84628-459-7_3).
37. Xiao, W., Photovoltaic power system modeling, design, and control, Wiely, Australia, (2017). (https://doi.org/10.1002/9781119280408).
38. Pavlovic., T., The Sun and photovoltaic technologies, Springer, University of Niš, Serbia, (2020). (https://doi.org/10.1007/978-3-030-22403-5).